Available online at www.sciencedirect.com
SCIENCE DIRECT®
Journal of Sound and Vibration 285 (2005) 1049–1070
JOURNAL OF SOUND AND VIBRATION
www.elsevier.com/locate/jsvi

Dynamic response of the Trinity River Relief Bridge to controlled pile damage: modeling and experimental data analysis comparing Fourier and Hilbert–Huang techniques

Ray Ruichong Zhang[a,*], Robert King[a], Larry Olson[b], You-Lin Xu[c]

[a]*Division of Engineering, Colorado School of Mines, Golden, CO 80401-1887, USA*
[b]*Olson Engineering, Inc., 5191 Ward Rd., Wheat Ridge, CO 80033, USA*
[c]*Department of Civil & Structural Engineering, Hong Kong Polytechnic University, Kowloon, Hong Kong*

Received 27 January 2003; received in revised form 7 September 2004; accepted 14 September 2004
Available online 12 January 2005

Abstract

This paper presents the implementation of a method for nonlinear, nonstationary data processing, namely the Hilbert–Huang transform (HHT) in traditional vibration-based approaches to characterizing structural damage and shows the frequency signature of local structural damage in nonstationary vibration recordings. In particular, following the review of traditional approaches to characterizing structural damage from nonstationary vibration recordings, this study first offers the justifications of the HHT as an alternative and complementary data process in addressing the nonstationarity of the vibration. With the use of recordings from controlled field vibration tests of substructures in the Trinity River Relief Bridge in Texas in its intact, minor- and severe-damage pile states, this study then shows that the HHT-based approach can single out some natural frequencies of the structure from a mixed frequency content in recordings that also contain the time-dependent excitation and noise frequencies. Subsequently, this study exposes that the frequency downshift for the damaged pile relative to the undamaged one is an indicative index for the damage extent. The above results are also validated by an ANSYS model-based analysis. Finally, a comprehensive HHT-based characterization of structural damage is discussed, and the potential use for cost-effective, efficient structural damage diagnosis procedures and health-monitoring systems is provided.

*Corresponding author. Tel.: +1 303 273 3671; fax: +1 303 273 3602.
E-mail address: rzhang@mines.edu (R.R. Zhang).

0022-460X/$ - see front matter © 2004 Elsevier Ltd. All rights reserved.
doi:10.1016/j.jsv.2004.09.032

1. Introduction

Bridge foundation damage from seismic and scour events should be assessed and/or monitored in a cost-effective manner so that catastrophic failures can be prevented, and corrective repairs can be carried out in a timely fashion. Water flow under bridges and earthquake-induced liquefaction causes loss of soil support around piers and abutments that will reduce the foundation's load-bearing capacity. The "unknown foundations" in over 100,000 bridges over water in the United States [1], however, imply that there is lack of cost-effective, efficient approaches to assess the damage caused by scour and liquefaction [2,3].

Several projects have measured and analyzed vibration responses to detect structural damage in general, and foundation damage in bridge substructures with simple geometries in particular [4–18], With a few exceptions, these projects applied a known excitation and recorded pre- and post-damage sets of large-array vibration data at multiple points. A change in dynamic characteristics (e.g., modal frequencies, shapes and damping) might identify damage location and severity. This approach has been proved technically feasible for many structures, but it generally requires a large and costly instrumentation system for data collection and the data analysis methods have not identified minor, local damage precursors to impending major damage [19].

In particular, the frequency response function (FRF), or modal vibration transfer function computed by the ratio of Fourier response amplitude spectra to excitation amplitude spectra, can identify vibration characteristics and subsequently quantify the change to structural damage. Recent studies [20–23] contend that the Fourier spectral analysis computes average, sometimes distorted, information, because it was intended to analyze stationary data, not the nonstationary data typical of structural response measurements. Fourier amplitude spectra define harmonic components globally producing average characteristics over the entire duration of the data. However, some characteristics of vibration data, e.g., the dominant frequencies, may change significantly with time. As a result, the averaging characteristic in Fourier spectral analysis such as FRF makes it insensitive for identifying time-dependent frequency content. Windowed (or short-time) Fourier spectral analysis corrects this problem, but it reduces frequency resolution as the length of the time window shortens. Thus, one is faced with a trade-off. The shorter the window, the better the locality of the Fourier amplitude spectra, but the poorer the frequency resolution. This influences the measurement of change of frequency resonance that typically arises in a low-to-intermediate frequency band typical of bridge foundation response.

Structural modal theory is widely used together with Fourier analysis for structural damage characterization. Local damage can be identified only through higher modes as shown by multiple-degree-of-freedom modeling of the whole structure. Determining the shape of the higher modes requires a large number of sensors, which makes data collection not only time consuming and expensive but also complicated (e.g., determining optimal locations of sensors). Typically the number of response measurement locations is significantly less than the number of degrees of freedom, which makes it difficult to precisely identify the change of local dynamic properties. Even with detailed data from large sensor arrays, it is difficult to distinguish local dynamic response from noise and excitation [20].

The Hilbert–Huang transform (HHT) [20,21] is applicable to nonlinear, nonstationary data and has found applications in solving classic nonlinear systems such as the Duffing equation to data

analysis in bio-engineering (e.g., blood-pressure variation), geophysics (e.g., ocean waves), and engineering (e.g., system identification) [22–32]. With the unique features of the HHT in nonstationary data processing, the implementation of HHT in the vibration-based approach for characterizing damage may not require such large sensor arrays and multiple recordings for damage detection. This study compares it with the Fourier technique in detecting local, minor damage with a computer model and experiments in two, pile bent foundations of the Trinity River Relief (TRR) Bridge. Consequently, this study contributes a comparative analysis of data from controlled destructive tests of a real structure. The study used a vibroseis truck to excite the structure and determines the effect of the excitation source on the frequencies of interest, which is inherently better than using unmeasured in situ vibration excitation, that is typically limited to the low-level response regime of the structure, or seismic data.

2. A method for nonlinear, nonstationary data processing

The HHT method builds on empirical mode decomposition (EMD) and Hilbert spectral analysis (HSA) [20,21]. HHT can decompose any complicated data set via EMD into a finite, often small, number of intrinsic mode functions (IMFs) that admit a well-behaved Hilbert transform. The IMF must meet two conditions: (1) the number of extrema and the number of zero-crossings must be equal or differ at most by one over the entire vibration-data time series; (2) the mean value of the envelope defined by the local maxima and the envelope defined by the local minima is zero at any point.

An IMF represents a simple oscillatory mode similar to a component in the Fourier-based simple harmonic function, but is more general. The EMD explores temporal variation in the characteristic time scale of the data and thus is adaptive to nonlinearity-related, nonstationary data processes. The HSA defines an instantaneous or time-dependent frequency of the data via Hilbert transformation of each IMF component. The above two steps of data processing (i.e., EMD and HSA) can represent vibration data $X(t)$ as

$$X(t) = \mathrm{Re}\left(\sum_{j=1}^{n} a_j(\omega, t)\mathrm{e}^{\mathrm{i}\int \omega_j(t')\,\mathrm{d}t'}\right), \tag{1}$$

where Re denotes the real part of the value to be calculated, the subscript j in both amplitude a_j and frequency ω_j indicates that the quantities are associated with the jth IMF component, i is the imaginary unit, e is exponential factor, and t and t' are times that bracket the jth IMF component. The amplitude a_j (ω,t) is designated as the Hilbert amplitude spectrum. Its square reveals the evolutionary energy distribution. The marginal amplitude spectrum, $h(\omega)$, defined as

$$h(\omega) = \sum_{j=1}^{n} \int_0^T a_j(\omega, t)\,\mathrm{d}t, \tag{2}$$

provides a measure of total amplitude or energy contribution from each frequency value, in which T denotes the time duration of data.

The HHT data representation can be compared with the Fourier representation of

$$X(t) = \mathrm{Re}\left(\sum_{j=1}^{N} A_j(\Omega)\mathrm{e}^{\mathrm{i}\Omega_j t}\right), \tag{3}$$

where A_j is the Fourier transform of $X(t)$, a function of time-independent frequency Ω. Specifically, the Hilbert amplitude spectrum $a_j(\omega,t)$ provides an extra dimension by including time t in motion frequency and is thus more general than the Fourier amplitude spectrum $A_j(\Omega)$. While the marginal amplitude spectrum, $h(\omega)$, provides information similar to the Fourier amplitude spectrum, its frequency term is different. Fourier-based frequency (Ω) is constant over the sinusoidal harmonics persisting through the data span or window, while HHT-based frequency ω varies with time, based on HSA over EMD-based IMFs. As the Fourier transformation window length reduces to zero, the Fourier-based frequency (Ω) approaches the HHT-based frequency (ω). Fourier-based frequency is locally averaged and not truly instantaneous since it depends on window length, which is controlled by the uncertainty principle and the data-sampling rate.

3. Vibration tests of intact, excavated and broken piles

Fig. 1(a) shows the TRR Bridge No. 4 on old US Hwy 90 west of Liberty, TX, where researchers conducted controlled damage experiments. TRR was built in the 1920s and consisted of four bridge structures. During the process of demolishing and replacing the bridge in 1996–1997, researchers selected the westernmost relief structure for dynamic testing. The structure had a 6.1 m (20 ft) wide roadway and consisted of 151 concrete panels directly supported by 66 concrete pile bents with a span of 5.5 m (18 ft). Bents 2 and 12 were tested because they had the same superstructures but different foundation types.

A portable field computer with a Data Physics (DP420) multi-channel FFT analyzer acquired data from PCB Model 393C seismic accelerometers mounted in 15 locations on columns and beams in each of the two bents in addition to a load cell that measured the excitation [3]. Fig. 1(a) also shows the University of Texas at Austin Geotechnical Engineering Center's vibroseis truck that generated the excitation forces. The truck's servo-hydraulic vibrator is capable of generating vertical dynamic forces above 311,374 N (70,000 pounds) over a frequency range from 1 to 120 Hz. The vibrator loading frame can contact the structure at single or dual points.

Data were initially gathered with the westernmost relief structure intact. Next, soil around Bent 12, containing sensor 15 (see Fig. 1(b)), was excavated back to the next pile, which simulated minor damage from flood-induced soil scour, causing partial loss of load-bearing capacity. Finally, Bent 12 was broken without replacing the excavated soil but leaving the steel-reinforcing bars, which simulated major damage from earthquake-induced shearing loss or severe scour causing complete loss of load-bearing capacity.

Bent 12 was comprised of a concrete beam cap supported by four, driven concrete piles. The beam cap was 7.2-m (23.5 ft) long × 0.6-m (2 ft) wide × 0.6 m high, while the piles had a 0.36 m (1.18 ft) square cross section. The beam cap was reinforced longitudinally with seven, number-7 steel bars and number-4 steel stirrups at 0.46-m spacing in the transverse direction. The concrete beam spanned 1.83 m (6 ft) symmetrically between the piles. Each pile had a, number-8 steel bar at

(a)

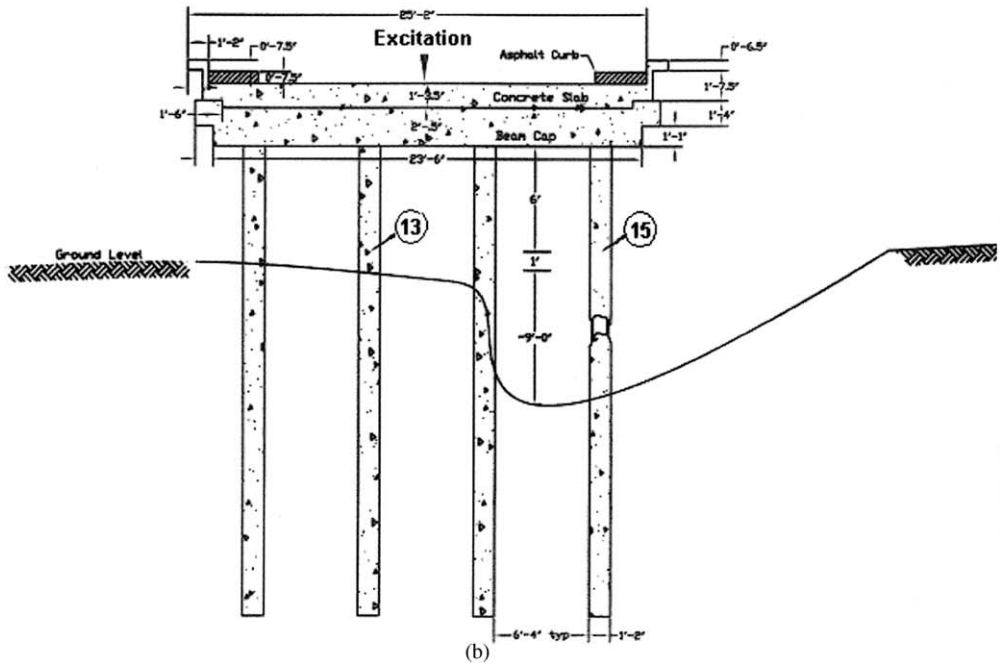

(b)

Fig. 1. (a) Relief Structure No. 4 of The TRR Bridge, Texas—vibroseis truck over Bent 12, and (b) The TRR Bridge Bent 12 structure with severe-damage state, i.e., soil around the pile with sensor 15 was excavated to the next pile, and the pile with sensor 15 was broken, leaving the steel-reinforcing bars only. The intact state of the structure is that the pile with sensor 15 was not broken, and soil around the pile with sensor 15 is at the ground level, the same height as the soil around the pile with sensor 13. The minor-damage state of the structure is that the pile with sensor 15 was not broken, but soil around the pile with sensor 15 was excavated to the same extent as the severe-damage state of the structure.

each corner of its cross section, with number-2 steel hoops at variable spacing from 0.05 m (0.16 ft) to 0.15 m (0.5 ft) along the pile. The exposed pile length between the bottom of the concrete beam and the ground surface was 2.1 m (7 ft), while the pile's total length was 7.62 m (25 ft).

4. Vibration analyses for intact to damaged piles

We will compare the HHT and Fourier techniques in the following, beginning with the Fourier analysis.

4.1. Fourier analysis of data from Bent 12

Fig. 2(a) and (b) shows, respectively, time histories of the vertical excitation force (forcing function) and resulting vertical (along-column) acceleration response at sensor 15 on Bent 12 in the intact state. The excitation force, and consequently the response, frequency swept almost linearly from 4 Hz at 0.3 s to 72 Hz at 5.7 s, referred to as a *chirp frequency* for later use. The Fourier amplitude spectra, shown in Fig. 3(a) and (b), gives average broadband frequency content of the data over the time period. The traditional alternative to chirp-frequency excitation is an impact force which results in similar broadband Fourier amplitude spectra. Fig. 3(c) presents the FRF (acceleration/force transfer function or accelerance), which can identify the natural

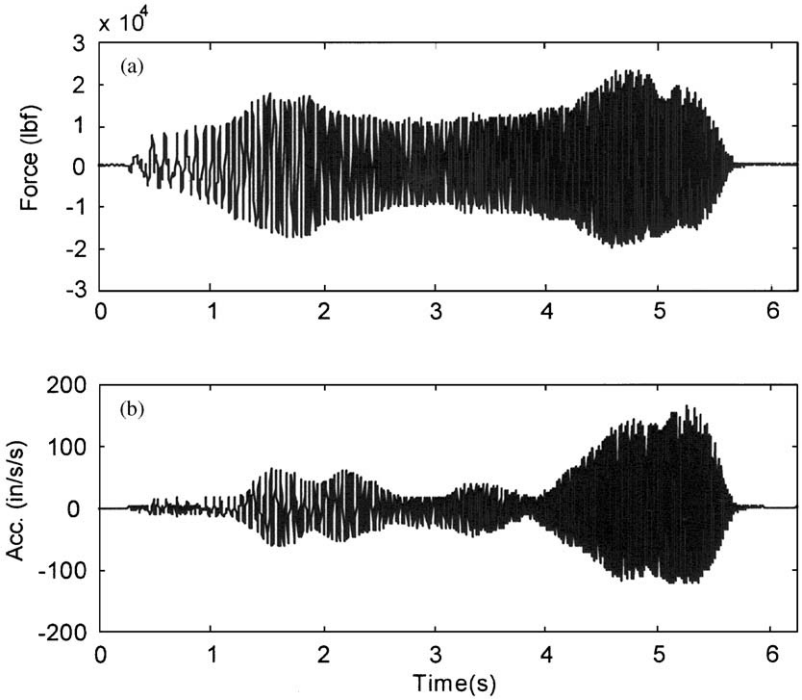

Fig. 2. (a) Forcing function and (b) recorded acceleration at sensor 15 with Bent 12 in the intact state.

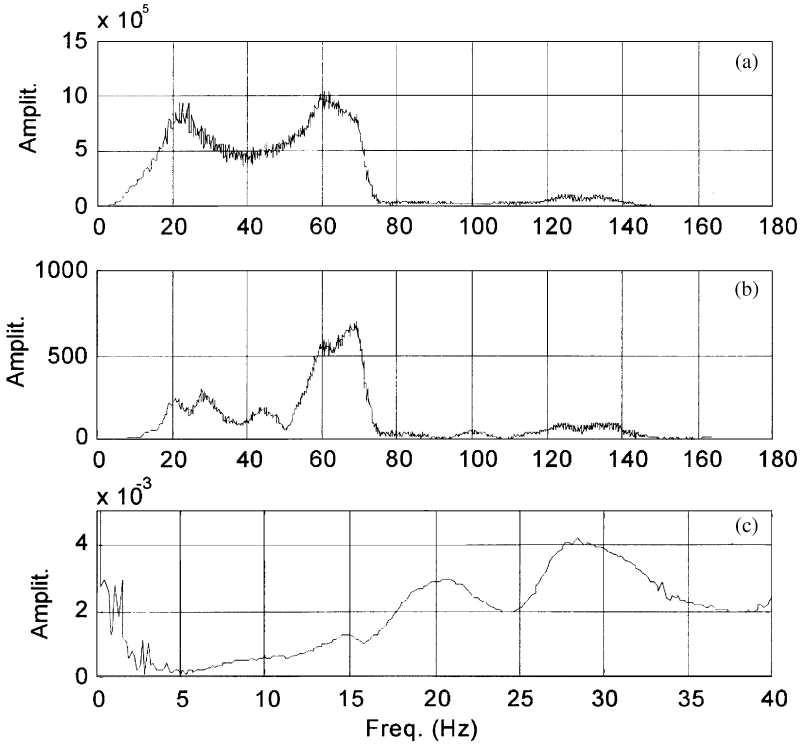

Fig. 3. Fourier amplitude spectra of (a) forcing function and (b) acceleration at sensor 15 with Bent 12 in the intact state, and (c) Fourier frequency response function at sensor 15 for Bent 12 in the intact state.

frequencies, damping, and modes. Fig. 3(c) shows the fundamental natural frequency to be 14.8 Hz at the first peak. Subsequent peaks represent second- and higher-order natural frequencies, but the peaks associated with frequencies lower than 5 Hz are probably caused by noise and vibration in other dimensions.

The 14.8 Hz fundamental natural frequency falls in the driving frequency range in the 0.5–2 s time period. Therefore, the response in Fig. 2(b) should contain a mix of the driving and fundamental natural frequencies, among others. The mixed frequency phenomenon exists only within the 0.5–2 s time band; therefore, the fundamental natural frequency identified from the global-based (or time-independent) Fourier-based FRF may not well distinguish the mixed frequency content.

While short-time Fourier spectral analysis can indeed aid in computing a local frequency dependent on the time instant of the selected window center, it may not essentially solve the dilemma of time–frequency resolution, i.e., getting accurate low-frequency information. Consequently, a short-time window FRF would not precisely identify low-order natural frequencies such as fundamental natural frequency in the current case. This is particularly true for the given excitation where the dominant frequencies are swept in a very short time interval [33].

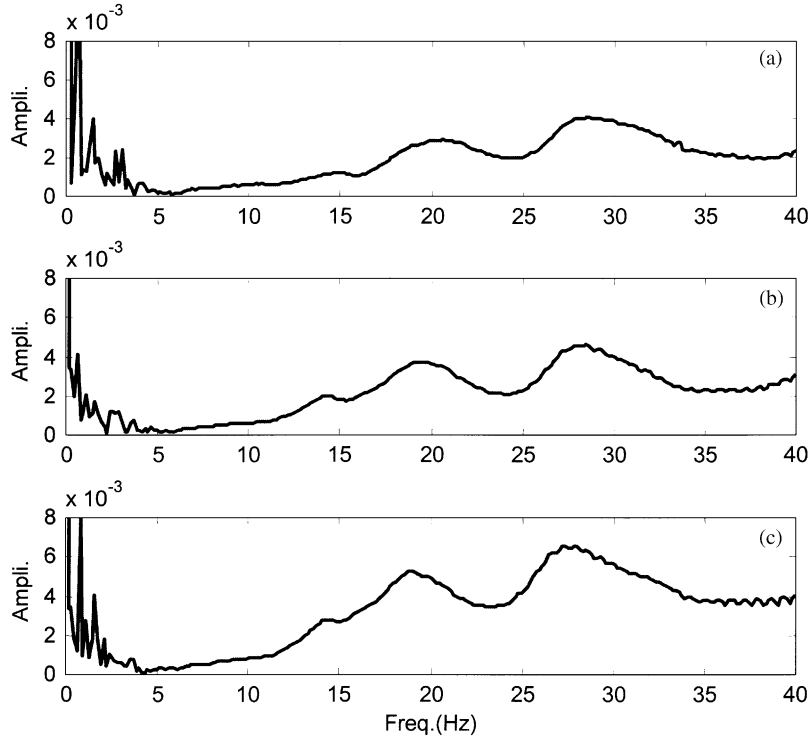

Fig. 4. Fourier frequency response functions at sensor 15 of Bent 12 in (a) the intact state, (b) the minor-damage state, and (c) the severe-damage state.

If a structural member has been damaged, the stiffness and thus the natural frequencies decrease as a function of the amount of damage. The damage may reduce the stiffness of a single member in a large structure without significantly affecting the stiffness of the entire structure. Consequently, vibration measurements on healthy members might not be sensitive to a small amount of localized damage elsewhere. Therefore, we expect to see frequency downshift in sensor 15 data since it was mounted on the damaged pile, but not at sensor 13 on the intact pile.

The fundamental frequencies in the minor- and severe-damage state FRFs at sensor 15, shown in Fig. 4(a–c), are only 6% and 9% lower than that in the intact state. The small downshift of the 2nd and 3rd natural frequencies and the increase of their corresponding amplitudes in the FRF are also observable in Fig. 4. Practically, such little change is difficult to distinguish from numerical error, thermal variation, or other effects, unless a comprehensive analysis of recordings at multiple locations is performed, which unfortunately was found to be problematic [3,34].

4.2. HHT analysis of data from Bent 12

Next, the HHT method was used to analyze the same data using the HHT Toolbox [35] for the EMD and HSA. The EMD was calculated using ten sifting operations and a 0–6 s data window. Around eight IMF components from each and every recording were extracted, each of which was

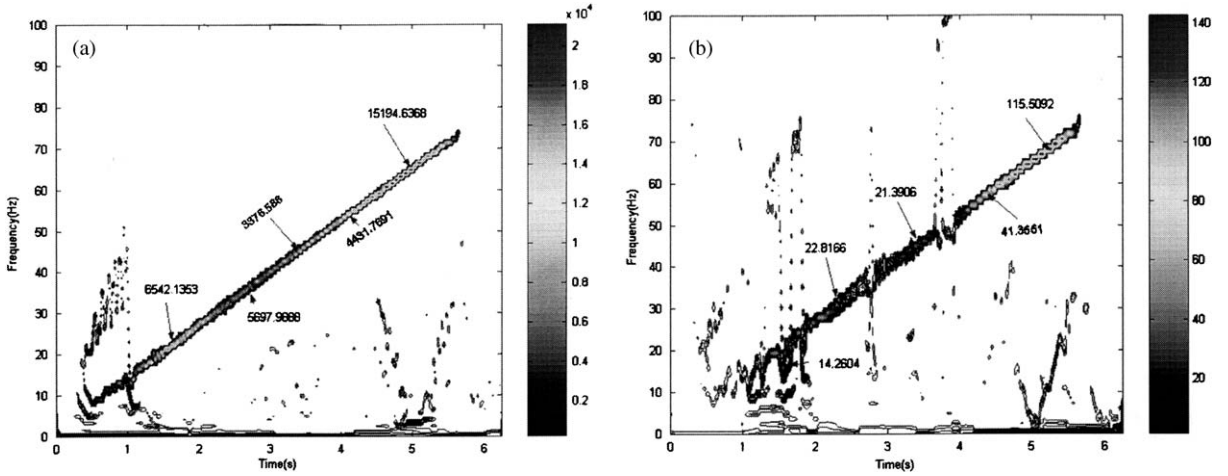

Fig. 5. Hilbert amplitude spectra of (a) forcing function and (b) acceleration at sensor 15 of Bent 12 in the intact state.

stable in terms of waveform, dominant-frequency band, and amplitude to secure stability of the subsequent Hilbert amplitude spectrum. Note that the EMD has end effects [20], which may affect local wave/vibration characteristics of the data set at two window edges and very-low frequency, high-order IMFs. Since the information extracted from the HHT focuses on frequencies above 1 Hz over a 1–2 s time band that is primarily related to the low- to intermediate-order IMFs, the end effects in the EMD sifting process are not critical to the problem at hand. Fig. 5(a) depicts the Hilbert amplitude spectrum of the excitation showing the chirp frequency almost linearly increasing from 4 Hz at 0.3 s to 72 Hz at 5.7 s (compare with Fig. 2(a)). The HHT graphs are three-dimensional, showing frequency (y-axis), time (x-axis), and amplitude (gray bar). The excitation energy at other frequencies such as high frequencies (20–50 Hz between 0.4 and 1.1 s) is also shown in Fig. 5(a) (note these frequencies in Fig. 2(a)).

Fig. 5(b) shows both the driving frequencies (e.g., chirp frequency) depicted in Fig. 5(a) and the natural frequencies of the structure. The energy in the 10–20 and 20–75 Hz frequency ranges between 1 and 2 s in Fig. 5(b) is attributable to the dynamic response signature of the structure. *This assertion, together with the subsequent interpretation, will be discussed further in Section* 5, *when we present the model-based analysis*. The 4–15 Hz excitation force between 0.4 and 1 s causes the 10–20 Hz vibration between 1 and 2 s (Figs. 2(a) and 5(a,b)). After 2 s, the 10–20 Hz structural vibration response (not the excitation) dies down quickly due to damping, and is too small to be shown in the figure in comparison with the strong excitation energy. Fig. 5(b) shows the fundamental natural frequency between 1 and 2 s, which is the first mode of vertical vibration motion dominant in the low-frequency band.

Fig. 6(a) provides a closer view of the Hilbert amplitude spectrum over the 0–3 s time interval. The structural dynamic response is shown in features other than the excitation-energy feature. The response-feature energy amplitudes use the same scale as in Fig. 5, with higher amplitudes shown by color infilling and lower amplitudes with no filling. The lowest frequency with a higher amplitude (infilling) is 12 Hz at 1.5 s, which is the fundamental natural frequency. It was caused by

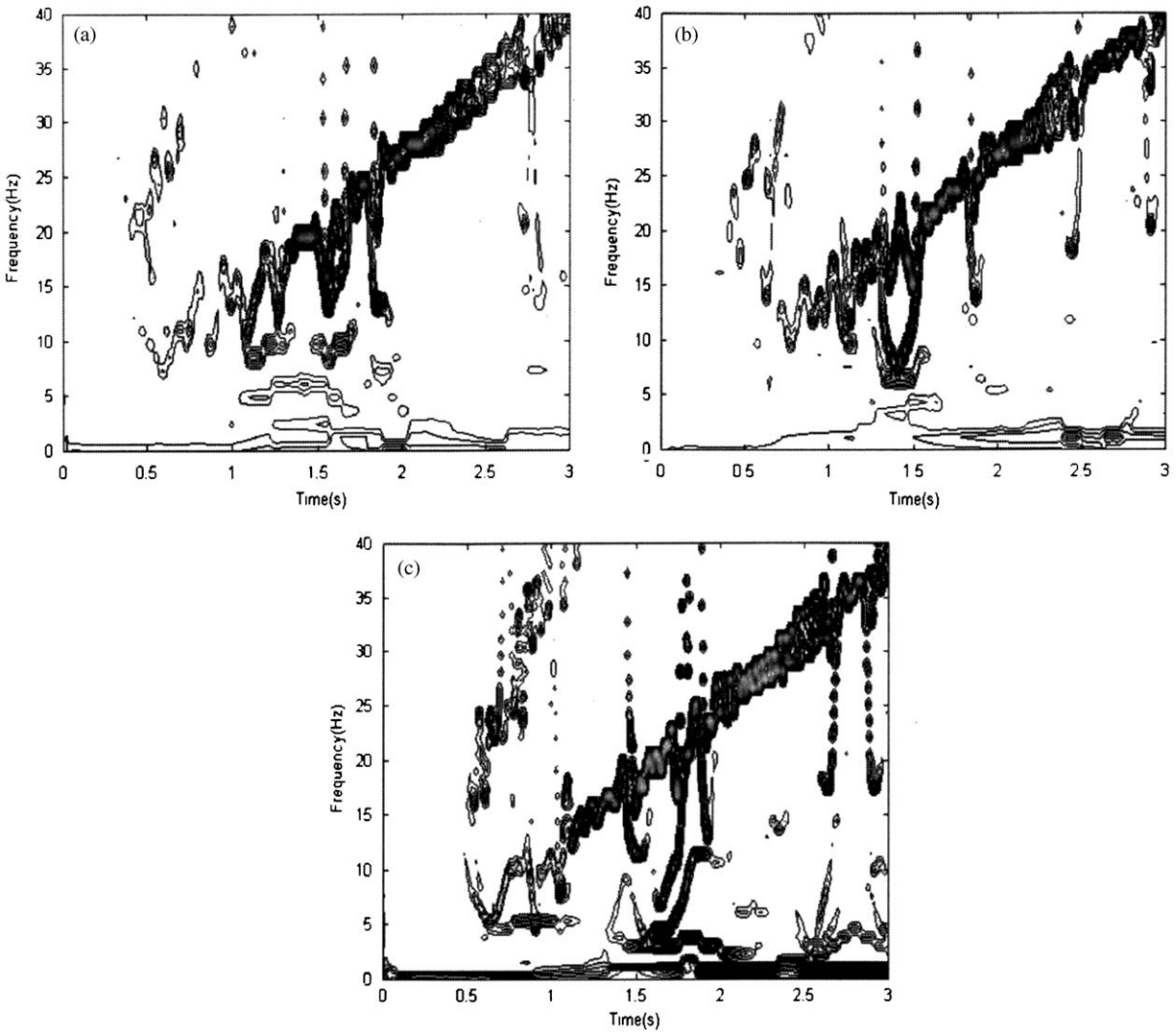

Fig. 6. (a) Hilbert amplitude spectra of acceleration at sensor 15 of Bent 12 in (a) the intact state, enlarged version of Fig. 5b, (b) the minor-damage state, and (c) the severe-damage state.

the 5–15 Hz excitation during the 0.4–1 s time interval. Fig. 6(a) also exhibits second- and higher-order natural frequencies and mixed frequencies.

In this case, the 12 Hz value is based on visual inspection. Test-to-test variability or environmental variability makes it difficult to compute an absolute fundamental frequency. Statistical analysis was considered to help in this respect, but limited destructive in situ vibration tests provide insufficient data sets for a statistical approach. Nevertheless, with the same criteria of visual inspection, the frequency downshift can be calculated from the relative spectra between the intact and damaged states in our study.

Fig. 6(b) shows the Hilbert amplitude spectrum of vibration response at sensor 15 with the bent in the minor-damage state (excavated soil). The response-energy dominant frequency fell to 6 Hz at 1.4 s. The dominant frequency decreased again to 3 Hz at 1.7 s in the severe-damage state (Fig. 6(c)). The responses could be related to the mixed natural frequencies of the bent and pile, since the vibration at sensor 15 should reflect the dynamic characteristics of both the whole bent and the local member. Soil excavation and concrete removal reduced the stiffness of the pile and thus lowered the fundamental natural frequencies of the bent and pile. This local-damage signature was not so clearly evident in the Fourier data analysis.

Fig. 7(a)–(c) shows the Hilbert amplitude spectra of vibration data at sensor 13 (on a case-independent intact pile). Fig. 7(a) shows that the dominant frequency is around 13 Hz at 2 s,

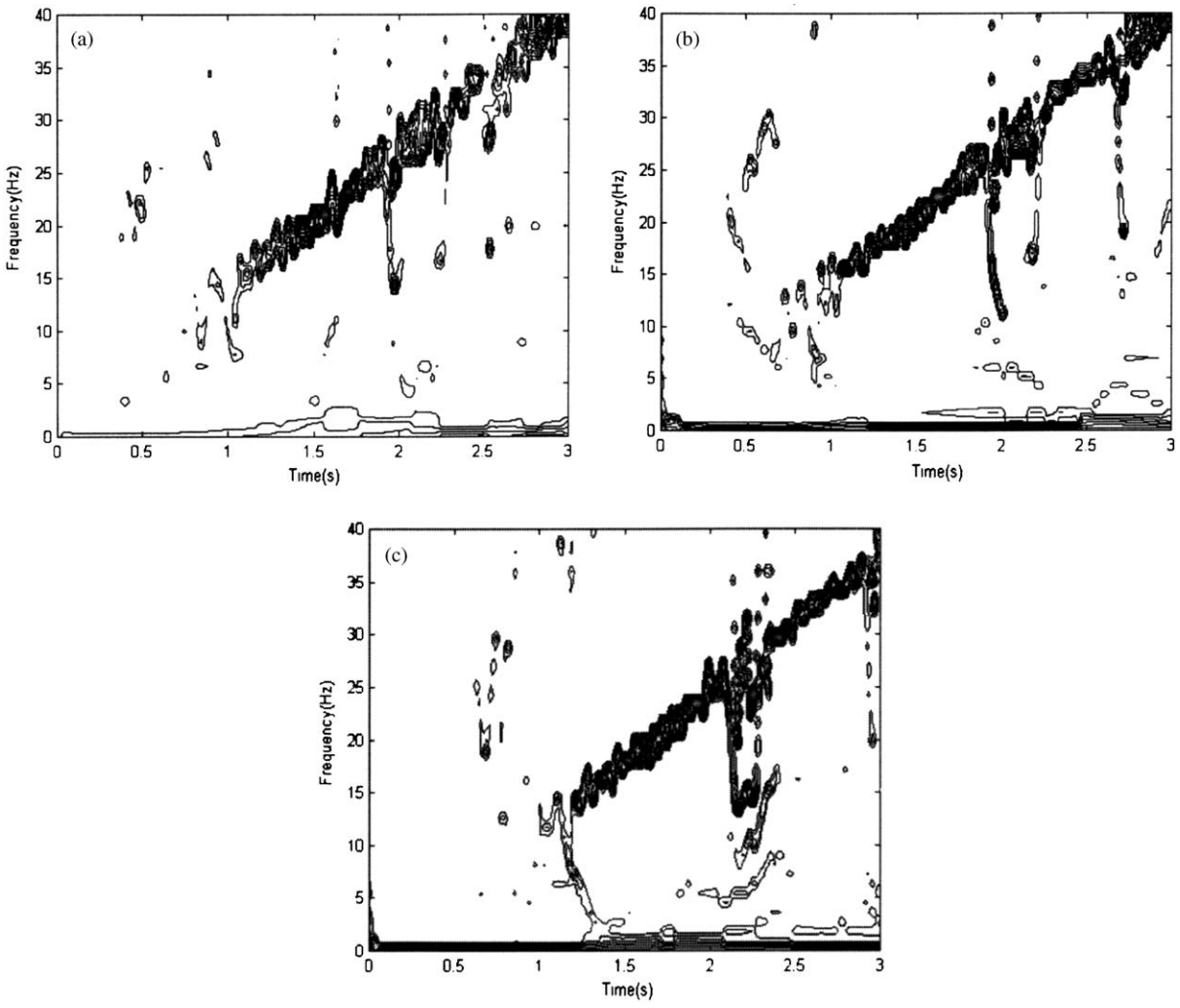

Fig. 7. Hilbert amplitude spectra of acceleration at sensor 13 of Bent 12 in (a) the intact state, (b) the minor-damage state, and (c) the severe-damage state.

slightly higher than 12 Hz identified from Fig. 6(a) which could be caused by noise and various uncertainties introduced when data were recorded. Fig. 7(b) and (c) shows the dominant structural vibration energy with a lowest frequency of 10 Hz at 2 and 2.2 s, respectively. Since sensor 13 is removed from the damage location, its vibration characteristics will retain primarily the dynamic features of the whole bent, which likely do not change significantly even with the local damage in the other pile. Thus, the sensor-13 dynamic-response spectra in Fig. 7(a)–(c) were relatively insensitive to the damage. Consequently, the HHT analysis showed a more significant frequency downshift than Fourier-based approaches for measurements made near the damage location or on the damaged member. This significantly improves practical efficiency in damage detection.

4.3. HHT analysis of data from Bent 2

To support the above analysis, we analyzed the data from sensors 9 and 11 on Bent 2 with the HHT technique. Fig. 8 shows the structural configuration of Bent 2 in the severe-damage state. Bent 2 is different from Bent 12 in that a shallow footing (0.6 m deep × 1.22 m wide) surrounds the structure's four piles at the ground surface and the sensors were located higher (closer to the beam cap) than sensors 13 and 15 in Bent 12. All the other conditions, including the field test setup, data collection and states of health and damage for the two bents, remain the same.

Fig. 9(a)–(c) shows the Hilbert amplitude spectra of vibration response at sensor 11 for the intact, minor- and severe-damage states, with fundamental natural frequencies of 10 Hz at 1.7 s, 7 Hz at 1.3 s, and 4 Hz at 1.2 s, respectively. Fig. 10(a)–(c) presents the Hilbert amplitude spectra of vibration response at sensor 9 (the intact pile) with frequencies of 13 Hz at 2 and 2.3 s, 12 Hz at 1.7 s, and 12 Hz at 1.9 s for the three states, respectively. The downshift of the fundamental natural frequency is consistent with the sequential damage and also similar to that in Bent 12. The difference of the fundamental natural frequencies between sensors 11 and 9 for the intact state could be attributed to the test-to-test or environmental variability, or the fact that the whole bent is not fully excited for a longer time period and therefore the recordings at each pile could reflect local-vibration characteristics more than whole-bent characteristics. Furthermore, since sensors 9 and 11 are, respectively, in the middle and side of four piles, the interior pile might possess more rigid local stiffness (combined footing/pile stiffness) and thus have a higher frequency than the exterior pile (less footing stiffness contribution).

5. Model-based validation

In order to confirm the observations in the last section and gain additional insight into HHT-based damage characterization, we conducted additional HHT analyses on simulated vibration data. Two-dimensional (2D) ANSYS finite-element-method (FEM) software models of Bent 12 in the intact and severe-damage states produced the simulated data. Inherent differences exist between FEM models and the real structure due to simplifications and assumptions about boundary and support conditions, connectivity between various structural elements, material properties, constitutive relationships (particularly those associated with soil and concrete), and

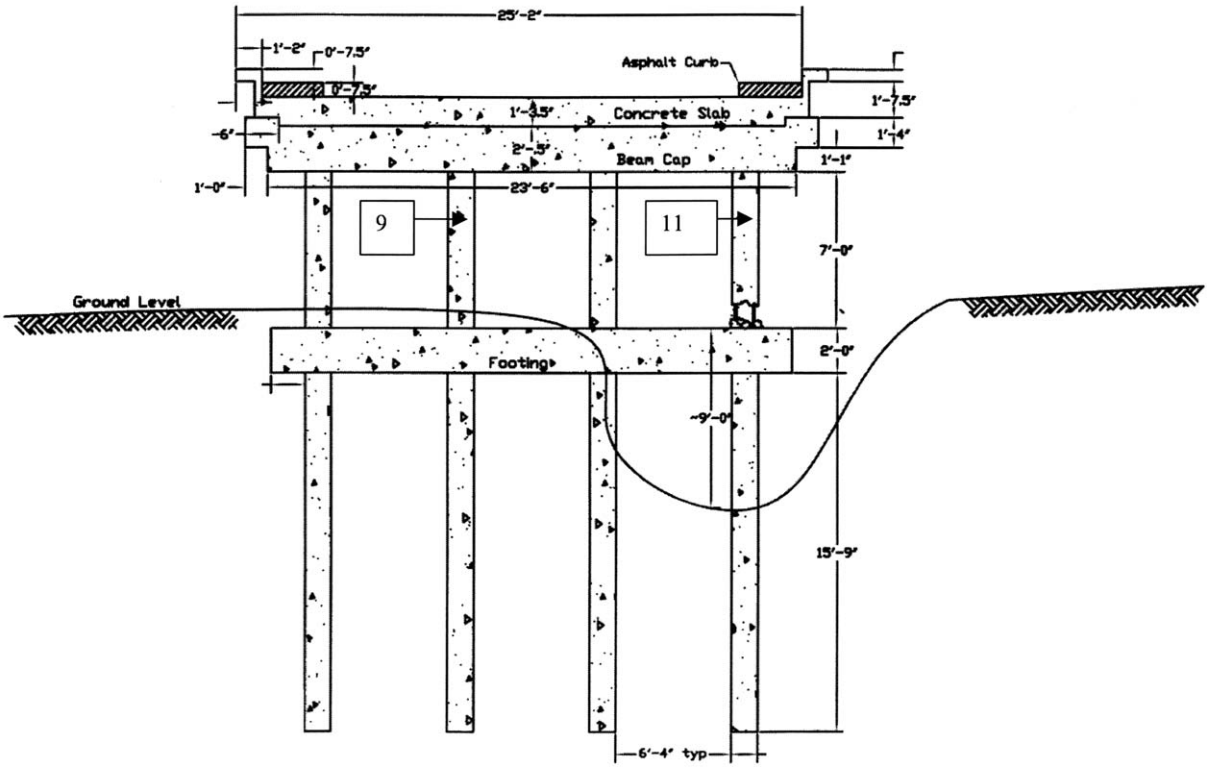

Fig. 8. The TRR Bridge Bent-2 structure with severe-damage state, i.e., soil above and below the footing around the pile with sensor 11 was excavated, and the pile with sensor 11 was broken at its bottom just above the footing, leaving the steel reinforcing bars only. The intact state of the structure is that the pile with sensor 11 was not broken, and soil around the pile with sensor 11 is at the ground level, the same height as the soil around the pile with sensor 9. The minor-damage state of the structure is that the pile with sensor 11 was not broken, but soil around the pile with sensor 11 was excavated to the same extent as the severe-damage state of the structure.

energy dissipation (damping) mechanisms. Therefore, the model-based approach provides useful information but it is limited.

5.1. ANSYS model for bent 12

The ANSYS-based 2D FEM model for Bent 12 in its intact state, shown in Fig. 11, was based on design specifications [34]. The dynamic characteristics of the 2D model provide sufficient information about the vertical dynamic characteristics pertinent to our study, so the additional complication of a 3D model was delayed for later studies [34]. The cap beams and columns of the bent were modeled with beam elements and were rigidly connected. The mass and stiffness of the bridge deck were lumped onto the cap beam, and the four piles were simply supported on the ground. The intact-state 2D model was extended to the severe-damage state by releasing the boundary restriction at the ground end of the sensor-15 pile (Fig. 11).

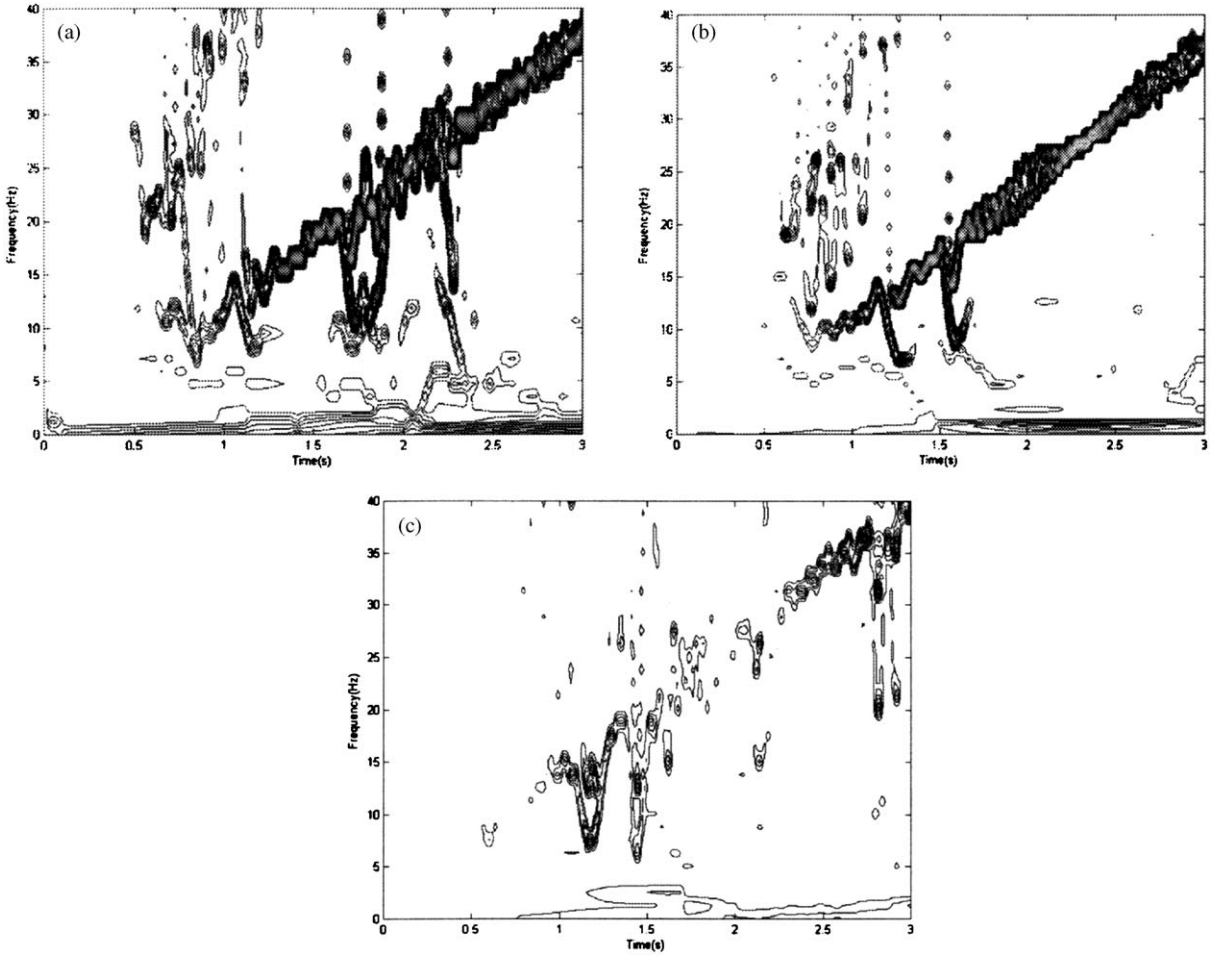

Fig. 9. Hilbert amplitude spectra of acceleration at sensor 11 of Bent 2 in (a) the intact state, (b) the minor-damage state, and (c) the severe-damage state.

Table 1 shows the first ten natural frequencies of the bent in the intact and severe-damage stages, identifying the first, second, and third natural frequencies in the vertical direction and their downshift percentage in the severe damage state.

The Rayleigh damping model simulated damping effects in the structure, according to the expression

$$[C] = a_0[M] + a_1[K], \tag{4}$$

where $[C]$, $[M]$, and $[K]$ are the damping, mass, and stiffness matrices, respectively, and a_0 and a_1 are the constant coefficients; additionally it was assumed that $a_0 = a_1 = d$, where d, the damping coefficient, was used [36].

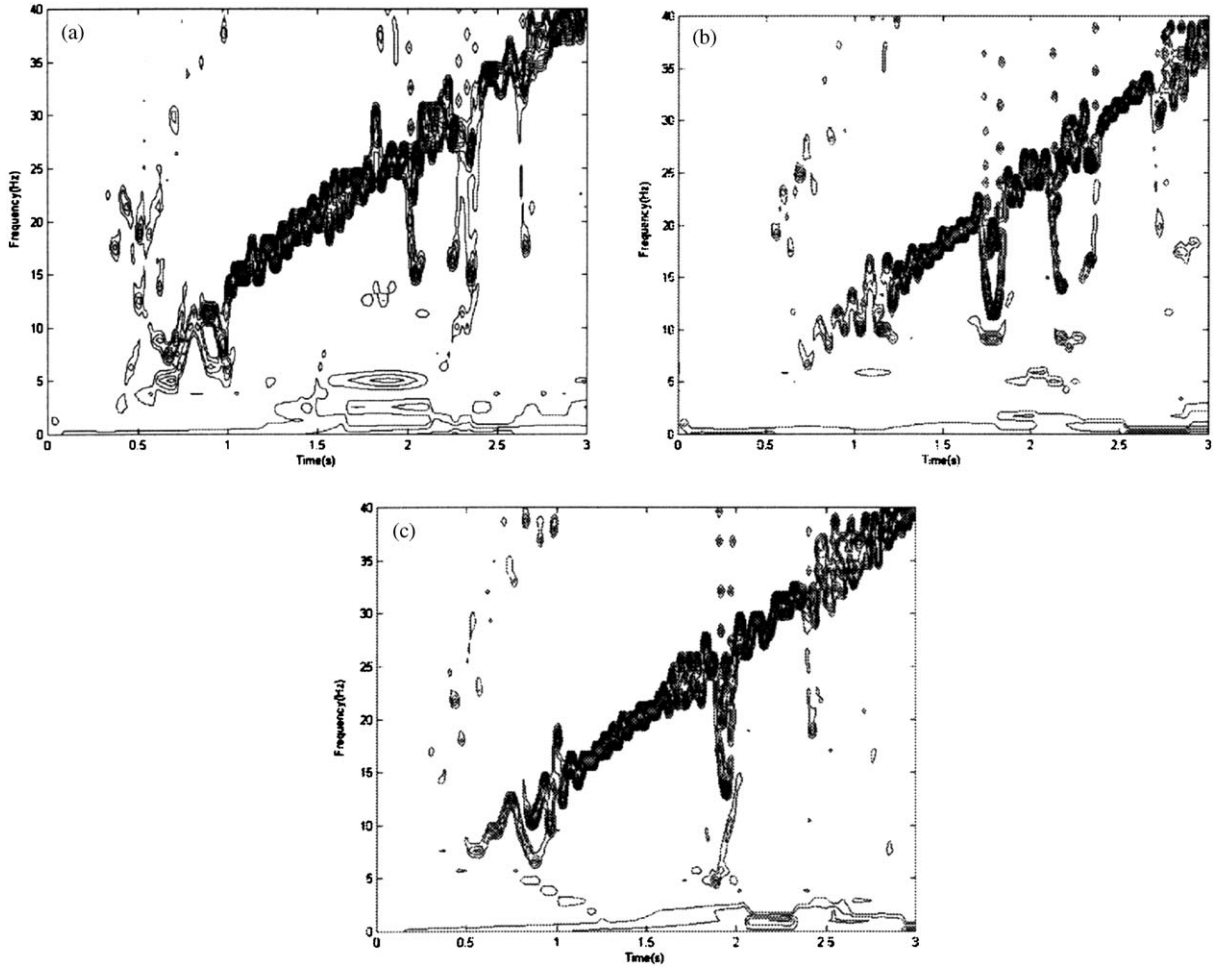

Fig. 10. Hilbert amplitude spectra of acceleration at sensor 9 of Bent 2 in (a) the intact state, (b) the minor-damage state, and (c) the severe-damage state.

5.2. HHT analysis of simulated data

Vibration responses were computed at nodes 37 and 53 (Fig. 11) that correspond to sensors 13 and 15 (Fig. 1(b)), respectively. Fig. 12(a) shows the Hilbert amplitude spectrum of the response at node 37 in the intact state with no damping, i.e., $d = 0$. The response energy is concentrated at frequency bands with their centers primarily around 12, 20, and 69 Hz, the first three modal natural frequencies in the vertical direction, respectively (see Table 1). This can be further clarified by examining the marginal amplitude spectrum in Fig. 13(a).

Without damping, the bent is fully excited at the natural frequencies. Therefore, the vibration energy at natural frequencies is typically higher than the excitation-inherited energy at chirp frequencies. Consequently, the energy inherited from the excitation at chirp frequencies is not

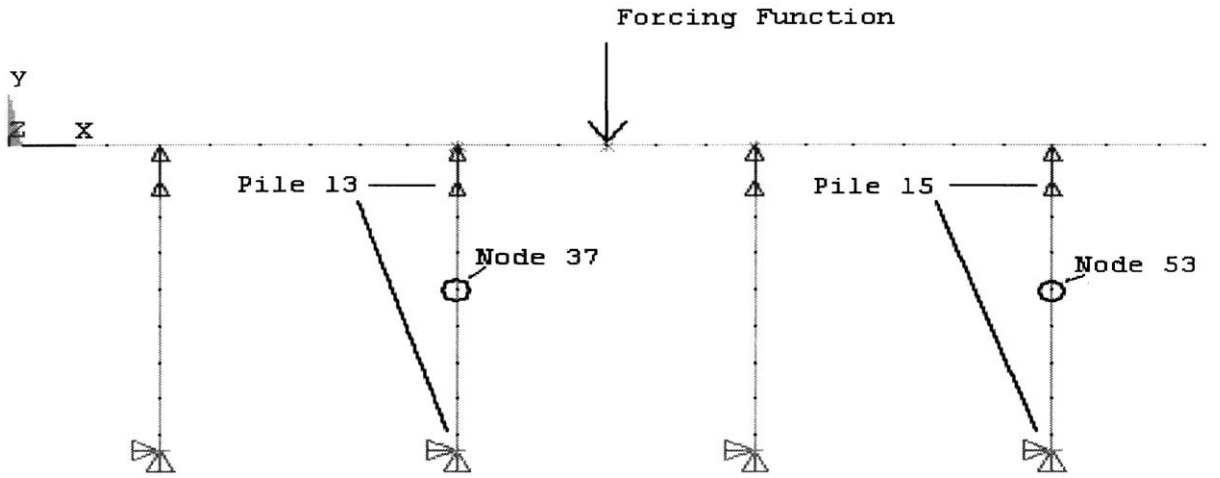

Fig. 11. ANSYS models for Bent 12 of TRR Bridge No. 4 in intact state. Piles 15 and 13, respectively, correspond to the piles with sensors 15 and 13 in Fig. 1(b).

Table 1
Fundamental natural frequencies from ANSYS model for Bent 12 in intact and severe-damage stages using design specifications

Natural frequencies in Hz (comments)	Intact	Severe damage (decrease w.r.t. intact)
1st	3.99	3.29
2nd (1st vertical natural frequency)	11.98	6.95 (41.98%)
3rd	14.84	12.47
4th (2nd vertical natural frequency)	19.68	18.08 (8.13%)
5th	44.01	39.19
6th (3rd vertical natural frequency)	69.22	52.50 (24.15%)
7th	93.88	72.50
8th	104.45	95.00
9th	106.37	105.82
10th	108.49	108.17

clearly shown in Fig. 12(a), except for the strong portion in the frequency band of 40–70 Hz at 3.5–5 s. With the damping, the relative intensity of the energy from the structure and excitation is changed, which can be seen from the Hilbert amplitude spectra in Fig. 12(b) and (c) with $d = 0.00198$ and 0.05305, respectively.

It is of interest to note that due to the strong input excitation and large damping, the second (and higher-order) natural frequencies are hardly observed from the structural response energy in Fig. 12(b) and (c), not as the first natural frequencies. This is primarily due to the amplitude resolution used in plotting Fig. 12(b) and (c). If the resolution in Fig. 12(b) and (c) is further lowered, the first natural frequency would not be observed from the figures. In contrast, the higher-order natural frequencies can often be observed in the Fourier amplitude spectra, with the

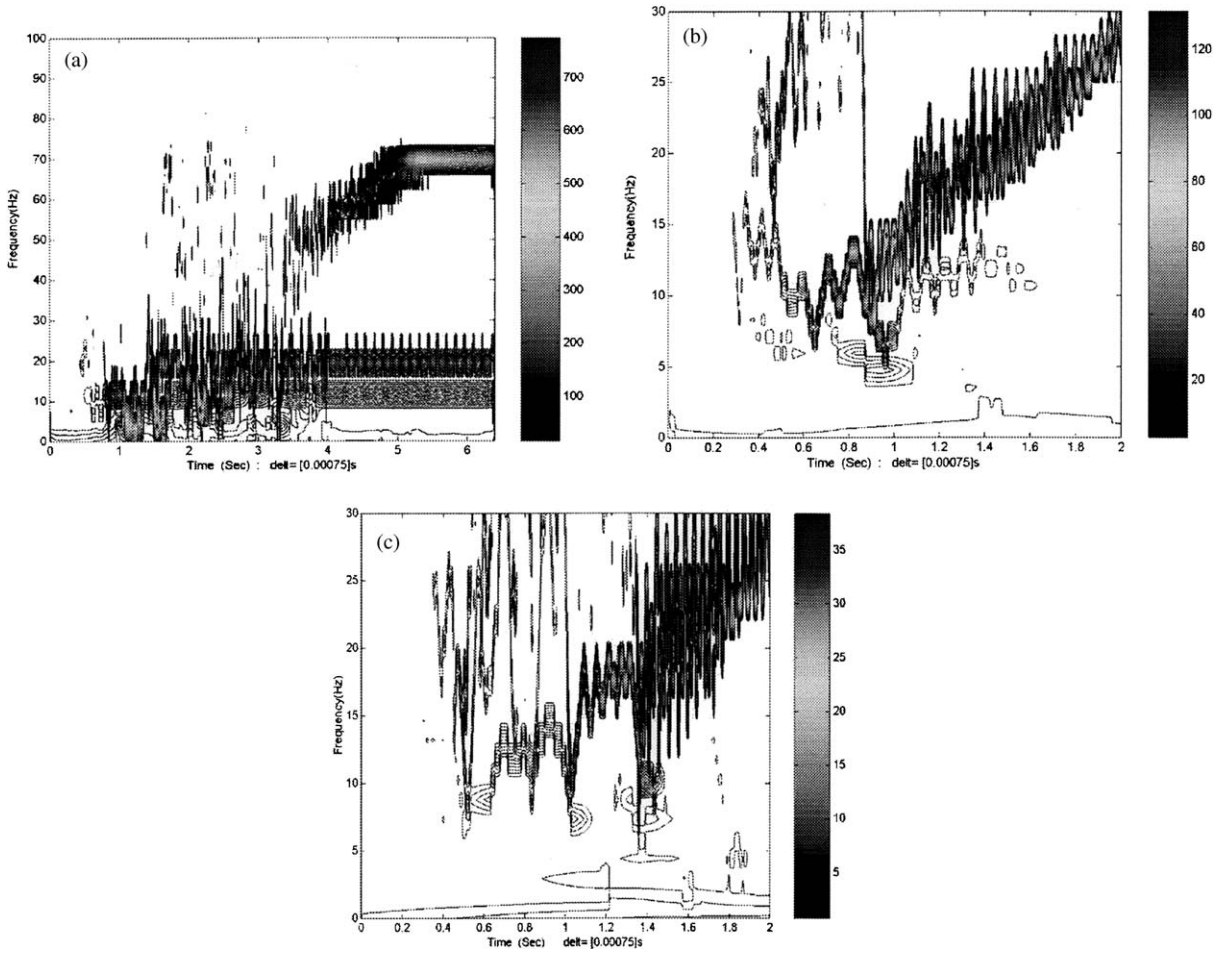

Fig. 12. (a) Hilbert amplitude spectra of acceleration at node 37 of Bent 12 in the intact state with (a) $d = 0$, (b) $d = 0.00198$, and (c) $d = 0.05305$.

aid of a logarithmic scale in amplitude. We believe that the higher-order natural frequencies can also be identified from the Hilbert amplitude spectra if the bar for the amplitude in Fig. 12(b) and (c) uses the logarithmic scale (not available now). On the other hand, the fundamental natural frequency and its change are of sole interest in this study. Therefore, this study will not further address the higher-order natural frequencies, although they can be an addition to the proposed identification.

The excitation-inherited energy in Fig. 12(b) includes the chirp frequency and the 10–30 Hz high-frequency band in the 0.3–0.8 s time interval, whereas the vibration energy falls in the 1–1.6 s time interval and 10–13 Hz frequency band. The marginal amplitude spectrum in Fig. 13(b) indicates that the first damped fundamental natural frequency in the vertical direction is around 11.5 Hz, smaller than the 11.98 Hz intact one in Table 1, indicating a small downshift. The vibration energy was greatly suppressed by the large damping and strong chirp-frequency

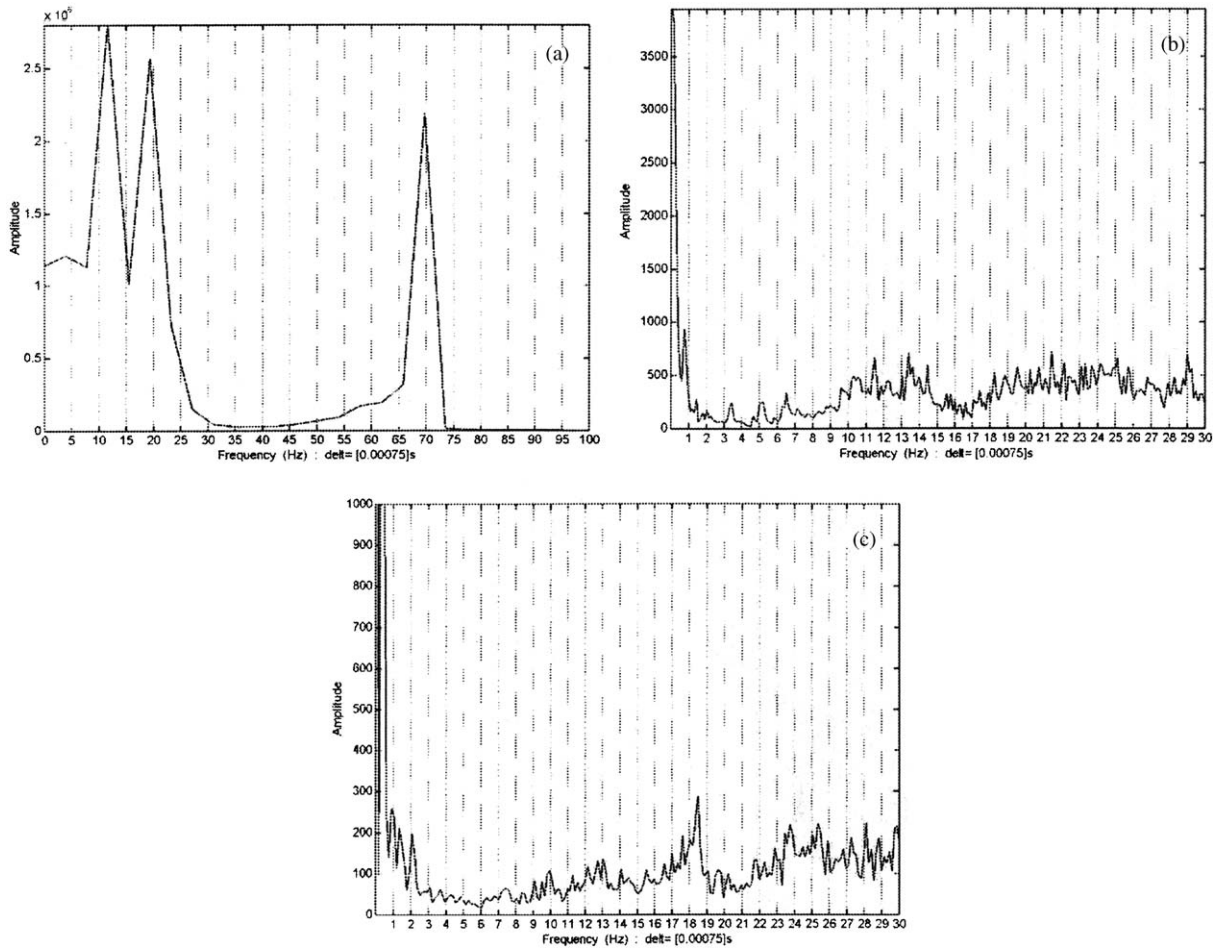

Fig. 13. (a) Marginal spectra of acceleration at node 37 of Bent 12 in the intact state with (a) $d = 0$, (b) $d = 0.00198$, and (c) $d = 0.05305$.

excitation, which is inherited with damping, in comparison to the real, intact case (Fig. 12(a) and (b)). Consequently, the vibration energy at 11.5 Hz in Fig. 13(b) is comparable to the energy at other frequencies. Fig. 12(c) exhibits even larger damping.

Fig. 12(c) shows the 10-Hz vibration energy at 1.4 s, which is also prominent in Fig. 13(c). Since the damping here is very high, the fundamental natural frequency is greatly downshifted from the 11.98-Hz intact one. These results were obtained by setting damping $d = 0.05305$ in the ANSYS model (Fig. 11) with generated time history responses similar to those in Fig. 2(b) [33]. This indicates that the real damping of Bent 12 was very high in the vertical direction, which can also be verified using the half-power (band-width) method [36].

Fig. 14(a) and (b), respectively, show the Hilbert response spectra at nodes 37 and 53 in the severe-damage state with $d = 0.03979$. Fig. 14(b) shows the vibration energy concentrates at 7 Hz from 0.5 to 1.2 s, i.e., the severe-damage fundamental natural frequency in Table 1. In contrast,

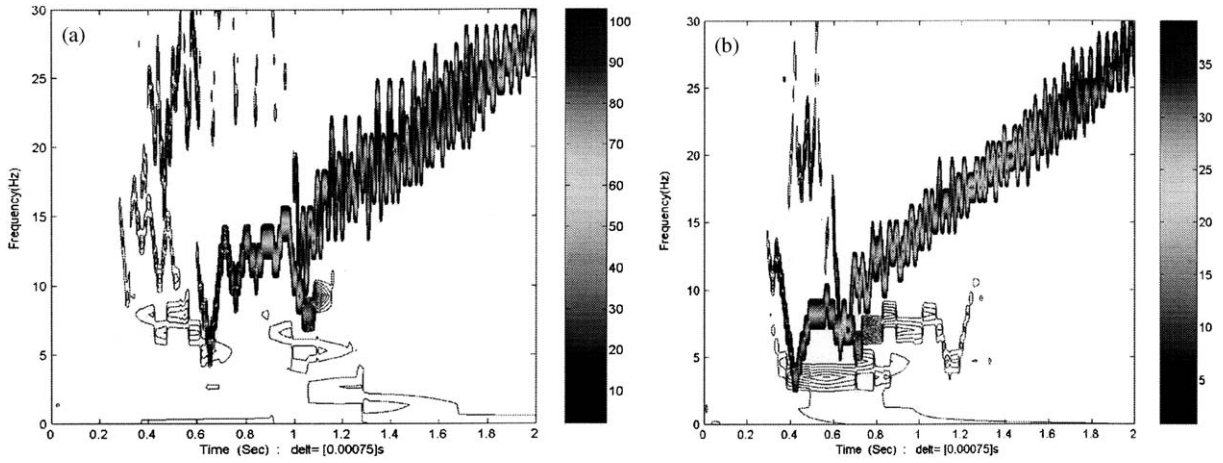

Fig. 14. Hilbert amplitude spectra of acceleration of Bent 12 in the severe-damage state with $d = 0.003979$ at (a) node 37 and (b) node 53.

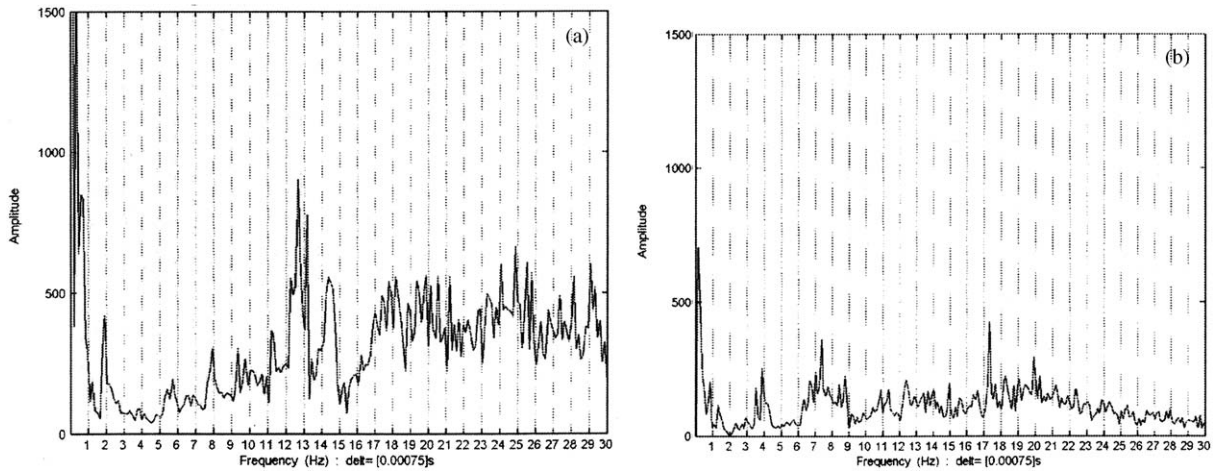

Fig. 15. Marginal spectra of acceleration of Bent 12 in the severe-damage state with $d = 0.003979$ at (a) node 37 and (b) node 53.

the dominant vibration energy in Fig. 14(a) is at around 12 Hz between 0.6 and 1 Hz and minor vibration energy at 7 Hz at 1 + s, which is also evident in the marginal amplitude spectra in Fig. 15(a) and (b). Comparison with the measured 7-Hz dominant response energy frequency in Fig. 12(a) and (b) helps identify qualitatively the damage location and severity.

6. Concluding remarks and discussion

This study compared the HHT analysis with traditional Fourier and modal transfer function data analysis techniques for identifying damage in bridge piles. It revealed that

the HHT technique identified local damage by comparing data from a sensor mounted on a damaged pile with sensor data from an intact pile. The HHT technique did not need the a priori data required in traditional damage diagnosis, and thus improved health-monitoring efficiency.

It should be pointed out that the presented HHT analysis of in situ data sets is difficult to visually identify the natural frequencies from the Hilbert amplitude spectra such as in Figs. 6 and 7. This could be due to the following reasons: (1) quality of data sets that could be influenced by the appropriate test setup, test-to-test variability, environmental variability, and noise; (2) proposed identification procedure for frequency and its downshift; and (3) the HHT method itself. To clarify the above issues, this study then shows the HHT analysis of simulated data sets with an ANSYS structural model. From the latter, one can identify the natural frequencies and corresponding downshift associated with the structural damage. This also implies that the ambiguous identification of frequency and its downshift from the in situ data sets is primarily related to the quality of the data sets, not to the proposed procedure and the HHT method itself.

It is also noted that the problem under investigation was stochastic. Therefore, establishment of statistical bounds for the identified or to-be-identified physical quantities (e.g., frequency) would improve the reliability of the damage detection and quantification. However, the limited number of available destructive in situ vibration tests provided insufficient data sets for a statistical approach. Consequently, the results and conclusions drawn from the study could be improved with additional data sets.

In addition, structural damage reduces material strength, increases damping, and consequently, changes the vibration mode. Therefore, comprehensive damage characterization and identification require the assessment of frequency downshift, damping, mode-shape change, and possibly waveform deformation and amplification. Multiple indices are typically needed since a single index like frequency downshift alone may not be adequate for practical use in locating and quantifying damage [3,34]. This will be the subject of further study.

While further work is needed for the comprehensive understanding and practical identification of damage, work to date suggests that the following process has potential for structural health monitoring and damage detection.

(1) Select two or more similar structural members (e.g., two of four columns in a bridge with the same size, cross section, and materials) for a non-destructive vibration test, and mount one sensor (e.g., accelerometer) on each. Apply a dynamic excitation at a location close to, but not in the members. Digitize and store the dual-channel sensor output with a computer data acquisition system.
(2) Decompose the two data sets into a number of IMF components using the EMD process, and feed them to the HSA to compute the Hilbert amplitude spectrum. Identify the driving frequency, natural frequency, and other frequency contents by analyzing the Hilbert spectra and IMF components.
(3) Compare the natural frequencies of the members to identify all frequency downshifts indicating that the lower-frequency members are more damaged than higher frequency members. If frequencies are the same, the members are equally damaged and a priori data from testing the same structure may be required.

Acknowledgments

The authors would like to express their appreciation for the financial support provided by the National Science Foundation (Grant Nos. 0085272 and 0414363) and by the Federal Highway Administration (Contract DTFH61-96-00030). Financial support is also acknowledged from the strategic research program of the Hong Kong Polytechnic University (HKPU) and the US-PRC Researcher Exchange Program administered by the Multidisciplinary Center for Earthquake Engineering Research. Thanks are also extended to Shou Ma and Matthew MacRostie, who helped provide some computational analyses in this study. The opinions, findings and conclusions expressed herein are those of the authors and do not necessarily reflect the views of the sponsors.

References

[1] E. Richardson, L. Harrison, Evaluating scour at bridges, FHWA-I-90-017, Hydraulic Engineering Circular No.18, 1993.
[2] P.F. Lagasse, P.L. Thompson, S.A. Sabol, Guarding against scour, *Civil Engineering Magazine*, 1995.
[3] L.D. Olson, Dynamic bridge substructure evaluation and monitoring system, *Report of FHWA Grant to Olson Engineering*, 2002.
[4] C.R. Farrar, S.W. Doebling, Lessons learned from applications of vibration based damage identification methods to large bridge structure, in: F.K. Chang (Ed.), *Structural Health Monitoring*: *Current Status and Perspectives*, Technomic Pub. Lancaster, PA, 1997, pp. 351–370.
[5] C.R. Farrar, S.W. Doebling, D.A. Nix, Vibration-based structural damage identification, *Philosophical Transaction of Royal Society of London, A*, 1999.
[6] C.R. Farrar, W.B. Baker, T.M. Bell, K.M. Cone, T.W. Dading, T.A. Duffey, A. Ekiund, A. Migliori, Dynamic characterization and damage detection in the I-40 bridge over the Rio Grande, *Las Alamos Report LA-12767-MS UC-906*, 15 June 1994, 3pp.
[7] O.S. Salawu, C. Williams, Bridge assessment using forced-vibration testing, *Journal of Structural Engineering* 121 (2) (1995) 161–173.
[8] O.S. Salawu, C. Williams, Review of full-scale dynamic testing of bridge structures, *Engineering Structures* 17 (2) (1995) 113–121.
[9] O.S. Salawu, Detection of structural damage through changes in frequency review, *Engineering Structures* 19 (9) (1997) 718–723.
[10] R. Ghanem, S. Sture, *Editorial, Journal of Engineering Mechanics* 126 (7) (2000) 665.
[11] J. Caicedo, S.J. Dyke, E.A. Johnson, Health monitoring based on component transfer functions, in: J.M. Ko, Y.L. Xu (Eds.), *Advances in Structural Dynamics*, vol. II, 2000, pp. 997–1004.
[12] F.K. Chang, *Structural Health Monitoring 2000*, Technomic, Lancaster, PA, 2000.
[13] G. Park, H.H. Cudney, D.J. Inman, Impedance-based health monitoring of civil structural components, *Journal of Infrastructure* 6 (4) (2000) 153–160.
[14] Z.Y. Shi, S.S. Law, L.M. Zhang, Optimum sensor placement for structural damage detection, *Journal of Engineering Mechanics* 126 (11) (2000) 1173–1179.
[15] A.W. Smyth, S.F. Masri, T.K. Caughey, N.F. Hunter, Surveillance of mechanical systems on the basis of vibration signature analysis, *Journal of Applied Mechanics* 67 (2000) 540–551.
[16] H. Sohn, J.A. Czarnecki, C.R. Farrar, Structural health monitoring using statistical process control, *Journal of Structural Engineering* 126 (11) (2000) 1356–1363.
[17] Y. Xia, H. Hao, Measurement selection for vibration based structural damage identification, *Journal of Sound and Vibration* 236 (2000) 89–104.
[18] J.M.W. Brownjohn, Ambient vibration studies for systems identification of tall buildings, *Earthquake Engineering and Structural Dynamics* 32 (2003) 71–95.

[19] J.N. Yang, P.C. Chang, H. Fujitani, H. Li, B.F. Spencer Jr., Y.L. Xu, F.G. Yuan, Structural control and health monitoring, *Proceedings of International Conference on Advances and New Challenges in Earthquake Engineering Research*, vol. 3, 2002, pp. 9–14.

[20] N.E. Huang, S. Zheng, S.R. Long, M.C. Wu, H.H. Shih, Q. Zheng, N-C. Yen, C.C. Tung, M.H. Liu, The empirical mode decomposition and Hilbert spectrum for nonlinear and nonstationary time series analysis, *Proceedings of Royal Society of London, A* 454 (1998) 903–995.

[21] N.E. Huang, Z. Shen, R.S. Long, A new view of nonlinear water waves—Hilbert Spectrum, *Annual Review of Fluid Mechanics* 31 (1999) 417–457.

[22] L.W. Salvino, Evaluation of structural response and damping using empirical mode analysis and HHT, *Fifth World Multiconference on Systemics, Cybernetics and Informatics*, July 22–25, Orlando, FL, 2001.

[23] R. Zhang, S. Ma, E. Safak, S. Hartzell, Hilbert–Huang transform analysis of dynamic and earthquake motion recordings, *Journal of Engineering Mechanics* 129 (8) (2003) 861–875.

[24] R. Zhang, S. Ma, S. Hartzell, Signatures of the seismic source in EMD-based characterization of the 1994 Northridge, California, earthquake recordings, *Bulletin of the Seismological Society of America* 93 (1) (2003) 501–518.

[25] K. Huang, A Nondestructive Instrument Bridge Safety Inspection System (NIBSIS) using a transient load, *US Patent Application number 09/210.693*; patent allowed April 2001.

[26] N.E. Huang, C.C. Chern, K. Huang, L.W. Salvino, S.R. Long, K.L. Fan, A new spectral representation of earthquake data: Hilbert spectral analysis of station TCU129, Chi-Chi, Taiwan, 21 September 1999, *Bulletin of Seismological Society of America* 91 (2001) 1310–1338.

[27] C.H. Loh, T.C. Wu, N.E. Huang, Application of the empirical mode decomposition-Hilbert spectrum method to identify near-fault ground-motion characteristics and structural responses, *Bulletin of Seismological Society of America* 91 (2001) 1339–1357.

[28] J.N. Yang, Y. Lei, Identification of tall buildings using ambient noisy wind vibration data, in: J.M. Ko, Y.L. Xu (Eds.), *Advances in Structural Dynamics*, vol. II, 2000, pp. 1093–1100.

[29] J.N. Yang, S. Lin, S. Pan, Damage identification of structures using Hilbert–Huang spectral analysis, *15th ASCE Engineering Mechanics Conference June 2–5*, Columbia University, NY, 2002.

[30] H.T. Vincent, S.L.J. Hu, Z. Hou, Damage detection using empirical mode decomposition method and a comparison with wavelet analysis, in: F.K. Chang (Ed.), *Structural Health Monitoring 2000*, 2000, pp. 891–900.

[31] T. Schlurmann, Spectral analysis of nonlinear water waves based on the Hilbert–Huang transformation, *Journal of Offshore Mechanics and Arctic Engineering* 124 (2002) 22–27.

[32] M. Niethammer, L.J. Jacob, Time–frequency representations of Lamb waves, *Journal of the Acoustical Society of America* 109 (2001) 1841–1847.

[33] M. MacRostie, Structural damage detection using advanced data processing and analysis, *MS Thesis*, Division of Engineering, Colorado School of Mines, Golden, CO, USA, 150, 2002.

[34] M. Sanayei, E.M. Santini, Dynamic bridge substructure evaluation and monitoring system, *Report of subcontract to Tufts University from FHWA Grant to Olson Engineering*, 1998.

[35] H. Huang, Transformation Toolbox, *Professional Edition V1.0*, Princeton Satellite Systems, Inc., Princeton, NJ, 2000.

[36] R.W. Clough, J. Penzien, *Dynamics of Structures*, second ed., McGraw-Hill, Inc., New York, 1993.